Multiphoton excitation and ionization of hydrogen atoms in two-color laser fields

Hong-Bin Yao [1,2] Zhao-Han Zhang,[1] Chen-Xi Hu,[1] and Feng He[1,3,*]

[1]*Key Laboratory for Laser Plasmas (Ministry of Education) and School of Physics and Astronomy,*
Collaborative Innovation Center for IFSA, Shanghai Jiao Tong University, Shanghai 200240, China
[2]*Key Laboratory of New Energy and Materials Research of Xinjiang Education Department,*
Xinjiang Institute of Engineering, Urumqi 830091, China
[3]*CAS Center for Excellence in Ultra-intense Laser Science, Shanghai 201800, China*

Using the hydrogen atom as a prototype, multiphoton excitation and ionization are simultaneously investigated with 400–800-nm laser fields. By tuning the relative phase ϕ between the two color components, the interference between different excitation channels results in the enhancement or suppression of the excitation probability and then determines the subsequent ionization. Moreover, the ϕ-dependent excitation and ionization are related to the relative intensity of the 400–800-nm fields. When the laser intensity of the 800-nm field is 5×10^{12} W/cm^2, the excitation and ionization probabilities present similar fluctuation behavior as a function of ϕ. With the increase of the 800-nm laser intensity, more multiphoton excitation and ionization channels open, and the ponderomotive energy begins to have an influence, making the two oscillatory behaviors differ from each other. The coexistence of excitation and ionization channels can be identified by decomposing the probabilities to the components with different angular quantum numbers, which can trace how the system absorbs multiphotons in strong laser fields and further control the ultrafast scenarios in atoms and even molecules.

I. INTRODUCTION

Advances in the development of laser technology have opened the possibility to observe ultrafast electron dynamics in atoms and molecules, which has attracted extensive research due to the possibility of a wide range of applications [1–8]. The dynamical information of the system is usually extracted by measuring photoelectron energy spectra (PES) of liberated electrons of atoms and molecules and the photoelectron momentum distribution (PMD) with strong-field photoelectron holography [9–11]. To provide explanations for the underlying mechanisms of the laser-driven electron dynamics, a series of theoretical methods have been developed, i.e., the exact solution of the time-dependent Schrödinger equation [12,13], numerical simulation within the strong-field approximation [14,15], theoretical calculation using the classical trajectory Monte Carlo [16–18] and quantum trajectory Monte Carlo [19] simulations, and so on.

The crucial step for studying strong-field ionization (SFI) is designing an ideal electric-field wave form to trigger and detect the ultrafast electron dynamics. Compared to the single-color field, two-color fields composed of a fundamental wave and its second harmonic offer a number of control parameters, such as polarization [20–22] and the relative intensity [22–25] between the two color components. In addition, the electric-field wave form can be tailored by tuning the relative phase of the two-color fields, which is more flexible for steering the electron motion in the ionization processes. In the past few decades, the research on SFI with two-color fields has

had considerable success. For example, using parallel polarized two-color (PTC) fields, the total ionization rate and a large forward-backward asymmetry in the emitted-electron distributions are controlled by manipulating the relative phase between the two color components [26–31]. In addition, information about ionization phases and time delays of electron wave packets formed in the ionization processes was uncovered by using the PTC fields [32–41]. With orthogonally polarized two-color (OTC) fields, the intercycle and intracycle interferences of different electron wave packets are disentangled in the measured PMDs, which can be spatially and temporally controlled by adjusting the relative phase of the OTC fields [42–47]. Moreover, the OTC fields have been used to probe the relative-phase delay and time delay in the photoelectron emissions of above-threshold ionization (ATI) [48,49]. Recently, using circularly polarized two-color (CTC) fields, the SFI and nonsequential double ionization were controlled efficiently by switching the relative helicity of the CTC fields [50–56].

Although the ionization in these two-color fields has been extensively studied, the excitation triggered by two-color fields has not been thoroughly discussed, probably because excitation cannot be directly measured in experiment. However, in multiphoton ionization scenarios, the excitation states are overwhelmingly important since the electron usually transits to excitation states by absorbing multiphotons, followed by ionization by further absorbing photons. Actually, atomic excitation is more complex than ionization since resonant excitation not only follows the fundamental rules, such as energy conservation and angular momentum conservation, but also depends on the laser parameters, such as polarization, frequency, and intensity [57–61]. Especially in intense laser

*fhe@sjtu.edu.cn

fields, the energy levels of excitation states are shifted by the laser field [62–64]. If two-color fields are simultaneously introduced into such processes, more parameters can be used to control the multiphoton excitation. More importantly, the coexistence of several excitation channels in two-color fields may interfere constructively or destructively, leading to the enhancement or suppression of the excitation [65,66], and may then affect the subsequent ionization.

Aiming at further exploration of the relative-phase-dependent excitation and ionization in the multiphoton regime, we investigate multiphoton excitation and subsequent ionization of hydrogen atoms with PTC fields. The modulation depths of the excitation and ionization probabilities are discussed for different relative intensities of the PTC fields. By decomposing the probability into components with different angular quantum numbers, the observed features of relative-phase-dependent excitation and ionization can be well explained. The rest of this paper is organized as follows. In Sec. II, we introduce the numerical method. The results and discussion are presented in Sec. III. The paper ends with a conclusion and outlook in Sec. IV.

II. NUMERICAL METHOD

The time-dependent Schrödinger equation (TDSE) for a single active electron under an external electric field in the dipole approximation using the velocity gauge can be written as (atomic units $e = \hbar = m = 1$ are used throughout unless otherwise stated)

$$i\frac{\partial}{\partial t}\Psi(\mathbf{r}, t) = \left[-\frac{\nabla^2}{2} + V(r) - i\mathbf{A}(t) \cdot \nabla\right]\Psi(\mathbf{r}, t), \quad (1)$$

where $V(r) = -1/r$ is the Coulomb potential of the hydrogen atom and the linearly polarized laser vector potential $\mathbf{A}(t)$ used in this paper can be written as

$$\mathbf{A}(t) = f(t)\left[-\frac{E_1}{2\omega}\sin(2\omega t) - \frac{E_2}{\omega}\sin(\omega t + \phi)\right]\mathbf{e}_z. \quad (2)$$

Here, ω is the angular frequency of the 800-nm laser field, E_1 and E_2 are the electric-field amplitudes of the 400- and 800-nm laser fields, and the pulse envelop $f(t) = \sin^2(\pi t/T_p)$ is adopted with a duration of $T_p = 20T_{400}$, with T_{400} being the period of the 400-nm laser field. The relative phase between the two color components is denoted by ϕ. In our calculations, the intensity of the 400-nm laser field is fixed at $I_1 = 5 \times 10^{13}$ W/cm^2, and the intensity of the 800-nm laser field I_2 varies from 5×10^{12} to 1.5×10^{13} W/cm^2.

Numerically, the time-dependent wave function $\Psi(\mathbf{r}, t)$ can be expanded with the basis of B-spline functions [67] and spherical harmonics,

$$\Psi(r, \theta, \varphi, t) = \sum_{j,l} c_{jl}(t)\frac{B_j(r)}{r}Y_l^{m_0}(\theta, \varphi), \quad (3)$$

where the expansion coefficients $c_{jl}(t)$ are time dependent and are obtained by diagonalizing the field-free Hamiltonian and then further propagated under the influence of the laser field. $B_j(r)$ are a set of B-spline functions, and $Y_l^{m_0}(\theta, \varphi)$ are the spherical harmonics. For the PTC fields, the magnetic quantum number is conserved and set to $m_0 = 0$. The

values of the radial index j and angular index l are integers extended from zero to $N_r - 1$ and zero to $N_l - 1$, where N_r and N_l are the numbers of B-spline functions and l partial waves, respectively. The angular index l represents the angular quantum number when $m = 0$ for the PTC fields, and the principal quantum number n satisfies the following transform: $n(l, j) = j + l + 1$.

Insertion of Eq. (3) into Eq. (1) yields the following matrix equation by imposing the Galerkin condition:

$$i\mathcal{S}\frac{d\mathbf{c}(t)}{dt} = [\mathcal{H}_0 + \mathcal{W}_z(t)]\mathbf{c}(t), \quad (4)$$

where $\mathcal{S}$ is the overlap matrix originating from the nonorthogonality of B-spline functions, $\mathcal{H}_0$ is the matrix of the field-free atomic Hamiltonian, and $\mathcal{W}_z$ is the atom-field interaction matrix. Detailed information about matrices $\mathcal{S}$, $\mathcal{H}_0$, and $\mathcal{W}_z$ can be found in Ref. [68].

Initially, the electron resides on the 1s state of a hydrogen atom. The corresponding wave function is obtained from the time-independent Schrödinger equation by diagonalizing the field-free Hamiltonian $H_0 = -\frac{\nabla^2}{2} + V(r)$ of the hydrogen atom, and the wave function propagation is performed using the Crank-Nicolson method together with the split-operator technique [68]. At the end of the laser pulses t_f, the probability for a certain bound nl state can be obtained by

$$P_{nl}^B = |\langle\psi_{nl}|\Psi(t_f)\rangle|^2, \quad (5)$$

where $\Psi(\mathbf{r}, t_f)$ is the final wave function and $\psi_{nl}(\mathbf{r})$ are the eigenstate states of the field-free Hamiltonian H_0 with energy $E_{nl} < 0$ [69]. The summation of P_{nl}^B with different l gives the probability of bound states with energy E_n, and the summation of P_{nl}^B with different n gives the probability of bound states with angular quantum number l. The total excitation probability is achieved by summing over all these populations on these nl states except for the 1s state.

The PES can be extracted by projecting the final wave function onto the exact scattering states of the hydrogen atom [68–70], which can be expressed as

$$P^I(\varepsilon) = \sqrt{2\varepsilon}\int|\langle\Phi_{\mathbf{k}}^-|\Psi(t_p)\rangle|^2 d\Omega_k, \quad (6)$$

where $\Phi_{\mathbf{k}}^-(\mathbf{r})$ is the eigenfunction of the atomic Hamiltonian with photoelectronic momentum $\mathbf{k} = (k, \Omega_k)$, and the energy of the liberated electron is $\varepsilon = k^2/2$. Alternatively, the PES can be obtained by summing over all the populations on each l partial spectrum,

$$P^I(\varepsilon) = \sum_l P_l^I(\varepsilon) = \sqrt{2\varepsilon}\sum_l |Z_l(\sqrt{2\varepsilon})|^2, \quad (7)$$

where $Z_l(k)$ is the l partial wave projection with momentum k [68]. The total ionization probability is achieved by integrating the PES over ε.

The TDSE is solved in a spherical box whose size is limited to $r_{\max} = 1000$ a.u. with time step $\Delta t = 0.008$ a.u. In our numerical calculations, we get converged results using a number of $N_l = 40$ with 1300 B-spline functions. The simulation box is large enough to hold all wave packets at the end of the calculation, and thus, no absorbing boundary conditions are needed.
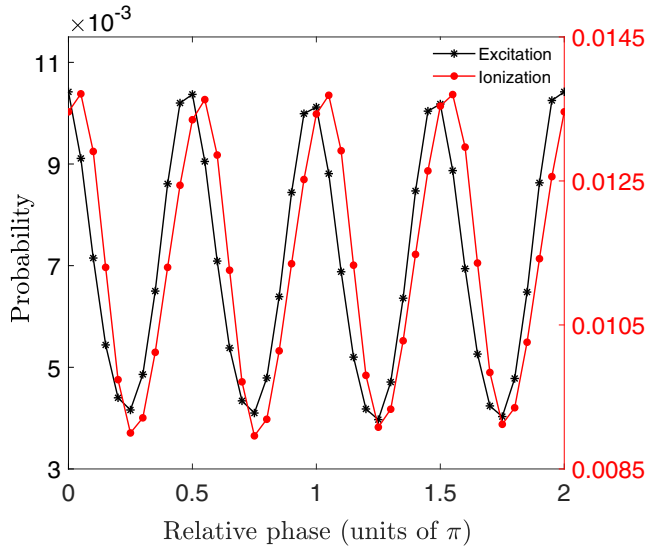
FIG. 1. The probabilities of excitation (black line) and ionization (red line) as a function of relative phase between the two color components. The laser intensities of the 400–800-nm fields are $I_1 = 5 \times 10^{13}$ W/cm^2 and $I_2 = 5 \times 10^{12}$ W/cm^2.

III. RESULTS AND DISCUSSION

We first look at the probabilities of excitation and ionization of a hydrogen atom in the 400–800-nm fields as a function of the relative phase ϕ, as shown in Fig. 1. One can see that both the excitation and ionization probabilities oscillate with the relative phase periodically. When the relative phase $\phi = n\pi/2$, the probabilities of excitation and ionization are maximum. When the relative phase $\phi = (2n + 1)\pi/4$, the probabilities of excitation and ionization are minimum. To characterize the relative-phase sensitivity of the excitation and ionization probabilities, we define the modulation depth Γ as [71]

$$\Gamma(\phi) = \frac{P_{\max}(\phi) - P_{\min}(\phi)}{[P_{\max}(\phi) + P_{\min}(\phi)]/2}, \qquad (8)$$

where $P_{\max}$ ($P_{\min}$) is the maximum (minimum) probability of excitation (ionization). As shown in Fig. 1, the modulation depths Γ of excitation and ionization are up to 90% and 42%, respectively. For reference, we also calculate the probabilities of excitation and ionization when only the 400-nm field is applied, in which case, the excitation and ionization probabilities are 0.0045 and 0.0237, respectively.

In order to understand the ϕ-dependent excitation probability, we decompose the excitation probability to each nl state. Figure 2 shows the probabilities of excitation states with a principal quantum number n and angular quantum number l by using different laser parameters. The contents of different panels are described in the caption. From Figs. 2(a) and 2(b), we find that hydrogen atoms are excited to the $n = 3$ state by absorbing four 2ω photons in the 400-nm monochromatic field, and the angular quantum number is primarily distributed on the $l = 2$ state. When the 800-nm laser field is added simultaneously, the excited atoms are mainly populated on the $n = 5$ state, as shown in Figs. 2(c) and 2(e). The multiphoton excitation channels can be deduced from the distribution of
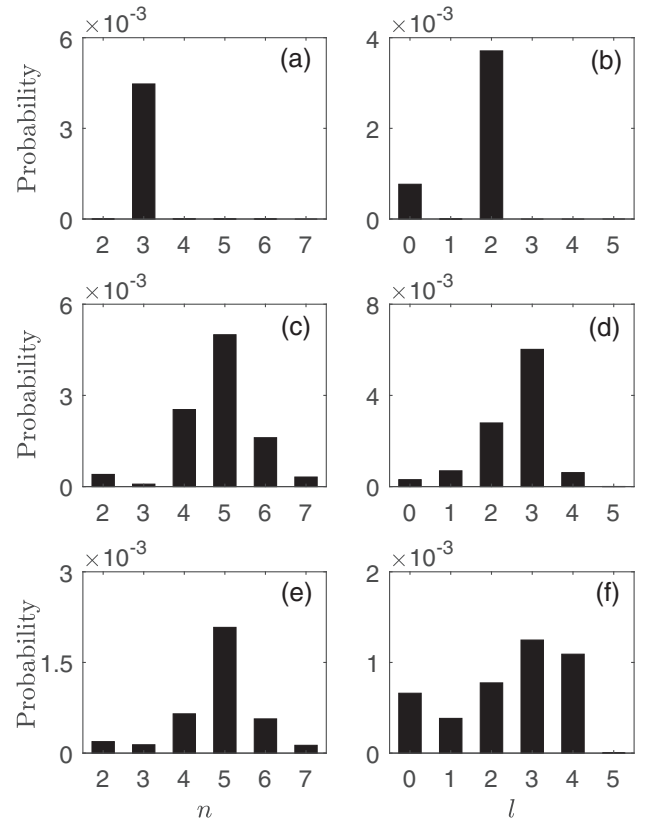

FIG. 2. The probabilities of hydrogen atoms on the nl excitation states in the 400-nm monochromatic field (top row) and the 400–800-nm fields with the relative phases $\phi = 0$ (middle row) and $\phi = 0.25\pi$ (bottom row). Left: The probability of excitation states with principal quantum number n calculated by summing over all the populations on each angular quantum number l. Right: The corresponding l partial probability calculated by summing over all the populations on each n. The laser intensities are the same as in Fig. 1.

atoms on each nl excitation state. According to the selection rule, one electron with an angular quantum number l can absorb a photon and consequently undergoes a transition $\Delta l = \pm 1$ [66]. Considering that the ground state of hydrogen is $1s$ state, only odd partial waves are populated when the hydrogen absorbs an odd number of photons, while the even partial waves are populated when the hydrogen absorbs an even number of photons [72]. For the relative phase $\phi = 0$ [Fig. 2(d)], the excitation of hydrogen is mainly distributed on the $l = 3$ state, but with an appreciable $l = 2$ contribution. Hence, we can deduce that the main channel of excitation is absorbing four 2ω photons and one ω photon. Alternatively, the atom can be excited by absorbing three 2ω photons and three ω photons. These two excitation channels interfere constructively to maximize the population of excitation states. When the relative phase becomes $\phi = 0.25\pi$ [Fig. 2(f)], the proportion of the excitation channel from absorbing three 2ω photons and three ω photons is relatively enhanced. In this case, the different excitation channels interfere destructively to minimize the population of excitation states.

After discussing the excitation process, we investigate the physical mechanism of ionization in the 400–800-nm fields. We calculate the PES, as shown in the left column of Fig. 3.
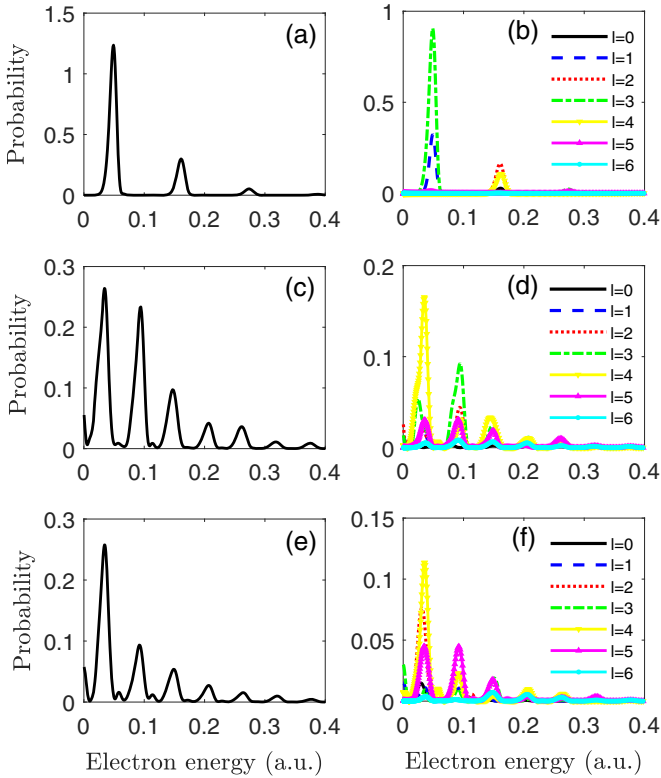
FIG. 3. The PES (left column) and the partial spectra for $l \leqslant 6$ (right column) in the 400-nm monochromatic field (top row) and the 400–800-nm fields with relative phases $\phi = 0$ (middle row) and $\phi = 0.25\pi$ (bottom row). The laser intensities are the same as in Fig. 1.
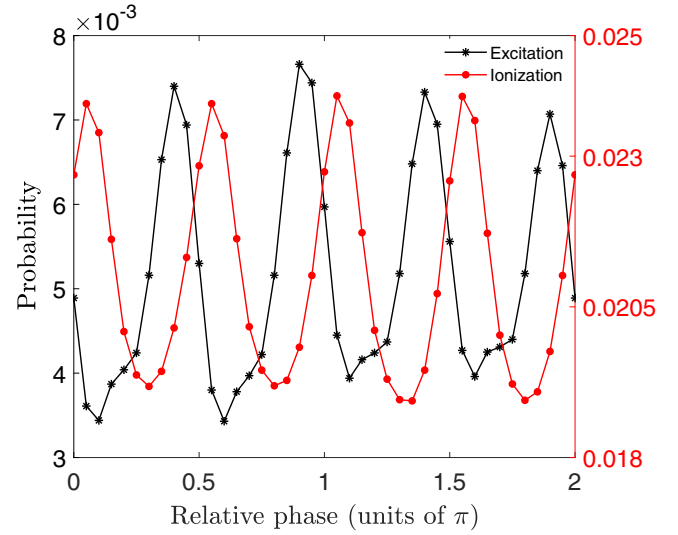

FIG. 4. The probabilities of excitation (black line) and ionization (red line) as a function of relative phase between the two color components. The laser intensities of the 400–800-nm fields are $I_1 = 5 \times 10^{13}$ W/cm^2 and $I_2 = 1 \times 10^{13}$ W/cm^2.

Further, we decompose the total PES to the l-resolved PES, as shown in the legend of Fig. 3. Here, only the $l < 7$ partial waves are counted since they contribute almost the total ionization probability. For the multiphoton ionization triggered by the sole 400-nm field, the ATI peaks locate at $E = n\hbar(2\omega) - I_p - U_p$ [62], with the ionization energy of hydrogen $I_p = 0.5$ a.u. and the ponderomotive energy $U_p = I_1/4(2\omega)^2$. This is, indeed, the case, as shown in Fig. 3(a). According to the partial spectrum of the 400-nm monochromatic field shown in Fig. 3(b), the first ATI peak exhibits a dominant angular momentum of $l = 3$, but with an appreciable $l = 1$ contribution since the partial wave of $l = 2$ is primarily populated on the excited state and, consequently, undergoes a transition $l \rightarrow l \pm 1$ by absorbing a 2ω photon. The single-photon absorption is inclined to populate on the partial spectrum with higher angular momentum l in the ionization process because the dipole transition from l to $l + 1$ is usually larger than the transition from l to $l - 1$ [73,74].

Switching on the ω field simultaneously, the ATI peaks are affected markedly. For the 400–800-nm fields with relative phase $\phi = 0$, the first ATI peak corresponds to the ionization from the $n = 5$ state by absorbing an ω photon, and the energy difference between these equidistant ATI peaks becomes $\Delta E = \hbar\omega$, as shown in Figs. 3(c) and 3(d). As already described in Figs. 2(c) and 2(d), the excited hydrogen is primarily populated on the $n = 5$ state with partial waves $l = 3$ and $l = 2$. Interacting with the 400–800-nm fields, the hydrogen can absorb an ω photon or 2ω photon in the contin-

uum states. For relative phase $\phi = 0$, the hydrogen atom on the $n = 5$ state with partial wave $l = 3$ is primarily ionized by absorbing an ω photon, and this state with partial wave $l = 2$ is mainly ionized by absorbing a 2ω photon. It can be deduced from Fig. 3(d) that the angular momentum composition of the first ATI peak contains 9% of the $l = 2$ character and 56% of the $l = 4$ character, and the second ATI peak contains 11% of the $l = 1$ character and 46% of the $l = 3$ character, which is very consistent with the propensity rule [75,76]. For relative phase $\phi = 0.25\pi$, shown in Figs. 3(e) and 3(f), the second ATI peak drops dramatically, and the main contribution of the partial spectrum $l = 3$ is replaced by the composition of $l = 5$. That is because the interference of the excitation channels gives rise to the wide range of the l distribution, and the population on partial wave $l = 3$ declines; the ionization of the 2ω photon absorption is mainly from partial wave $l = 4$.

When the laser intensity of the 800-nm field increases, the dynamic processes of excitation and ionization change dramatically, which leads to the variation of the modulation depths of excitation and ionization. Figure 4 displays the probabilities of excitation and ionization as a function of relative phase when the laser intensity of the 800-nm field increases to $I_2 = 1 \times 10^{13}$ W/cm^2. Compared with the case of using laser intensity $I_2 = 5 \times 10^{12}$ W/cm^2, the variation of the dissociation and ionization probabilities with the relative phase is no longer synchronized. The maximum excitation appears at relative phase $\phi = n \times \frac{\pi}{2} + 0.4\pi$, and the minimum appears at $\phi = n \times \frac{\pi}{2} + 0.1\pi$, while the maximum ionization appears at relative phase $\phi = n \times \frac{\pi}{2} + 0.1\pi$ and the minimum appears at $\phi = n \times \frac{\pi}{2} + 0.3\pi$. Tuning the relative phase of the 400–800-nm fields, the modulation depths Γ of excitation and ionization change to 76% and 24%, respectively. Because the contribution of the excitation channel caused by absorbing three 2ω photons and three ω photons is enhanced with the increase of the 800-nm laser intensity, it can influence the interference of different channels, leading to the variation of ϕ-dependent excitation and ionization. More importantly, the
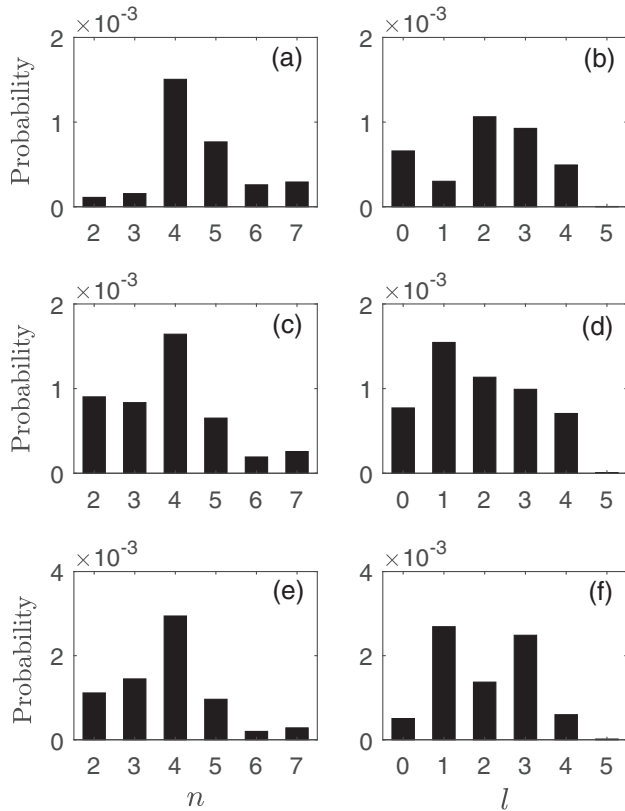
FIG. 5. The probabilities of hydrogen atoms on the nl excitation states in the 400–800-nm fields with relative phases $\phi = 0.1\pi$ (top row), $\phi = 0.3\pi$ (middle row), and $\phi = 0.9\pi$ (bottom row). Left: The probability of excitation states with principal quantum number n calculated by summing over all the populations on each angular quantum number l. Right: The corresponding l partial probability calculated by summing over all the populations on each n. The laser intensities are the same as in Fig. 4.
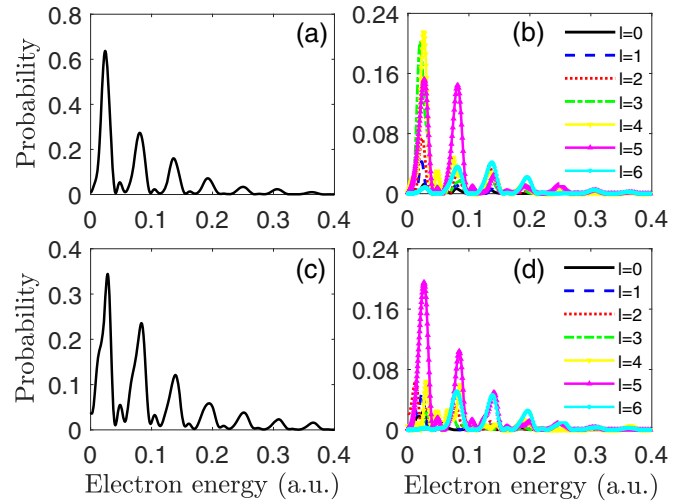

FIG. 6. The PES (left column) and the partial spectra for $l \leqslant 6$ (right column) in the 400–800-nm fields with relative phases $\phi = 0.1\pi$ (top row) and $\phi = 0.3\pi$ (bottom row). The laser intensities are the same as in Fig. 4.

ponderomotive energy U_p contributed by the 800-nm field is enhanced with the increasing 800-nm laser intensity. In this case, the energy levels of the excitation states are shifted by the 800-nm field, and then the distribution of these nl states changes, which may affect the subsequent ionization. In the following, we will discuss ϕ-dependent excitation and ionization at laser intensity $I_2 = 1 \times 10^{13}$ W/cm^2 in detail.

Figure 5 presents the probabilities of hydrogen atoms on the nl excitation states in the 400–800-nm fields with laser intensities $I_1 = 5 \times 10^{13}$ W/cm^2 and $I_2 = 1 \times 10^{13}$ W/cm^2. With the increase of the 800-nm laser intensity, the ponderomotive energy U_p contributed by the 800-nm field is up to 0.02 a.u., which is comparable to the photon energy and thus cannot be neglected. At $\phi = 0.1\pi$, the excitation probability is primarily contributed by the $n = 4$ state [see Fig. 5(a)]. The main channel of excitation is still absorbing four 2ω photons plus one ω photon; however, the channel from absorbing three 2ω photons and three ω photons is more pronounced. This results in the wide distribution of the angular quantum number, as confirmed in Fig. 5(b). Shifted by the ponderomotive energy in these 400–800-nm fields, single ω-photon ionization is possible only when the hydrogen atom populates on the $n \geqslant 4$ states according to the energy conservation. For relative

phase $\phi = 0.1\pi$, the atoms are mostly distributed on the $n \geqslant 4$ states. Since hydrogen atoms on these states are easily ionized by absorbing an ω photon, the excitation probability is the minimum while the ionization is the maximum at $\phi = 0.1\pi$. For $\phi = 0.3\pi$ and 0.9π, as shown in Figs. 5(c) and 5(e), the ac Stark effect shifts the $n = 2$ and $n = 3$ states into resonance. Compared with the case for $\phi = 0.1\pi$, many more atoms are distributed on the $n \leqslant 3$ states, which are difficult to ionize by absorbing an ω photon. Therefore, the excitation probability is the maximum at $\phi = 0.9\pi$.

In the plots in Fig. 6, we display the PES and corresponding partial spectra for $l \leqslant 6$ at laser intensities $I_1 = 5 \times 10^{13}$ W/cm^2 and $I_2 = 1 \times 10^{13}$ W/cm^2. For relative phase $\phi = 0.1\pi$, as shown in Figs. 6(a) and 6(b), the first ATI peak contains an extensive contribution in the partial spectrum $l \leqslant 5$. It can be deduced that hydrogen atoms on excitation states with partial waves $l \leqslant 4$ can be easily ionized by absorbing an ω photon. While the second ATI peak exhibits a dominant partial spectrum of $l = 5$, as we discussed above, it is mainly derived from the ionization of the 2ω photon absorption on excitation state $n = 4$ with partial wave $l = 4$, which corresponds to the excitation channel caused by absorbing three 2ω photons and three ω photons. The superposition of these ionization channels gives rise to the enhancement of ionization. At $\phi = 0.3\pi$, as shown in Figs. 6(c) and 6(d), the first and second ATI peaks exhibit a dominant partial spectrum of $l = 5$. They mainly come from the ionization of the excitation states with partial wave $l = 4$. The ionization from other partial waves is suppressed, leading to the minimum ionization probability at $\phi = 0.3\pi$.

According to Figs. 3 and 6, the ϕ-dependent ATI peaks also change with the laser intensity of the 800-nm field. As the laser intensities of the 400–800-nm fields are $I_1 = 5 \times 10^{13}$ W/cm^2 and $I_2 = 5 \times 10^{12}$ W/cm^2, as shown in the Fig. 7(a), the maximum of the first ATI peak appears at relative phase $\phi = n \times \pi/2 + 0.1\pi$. This is caused by the interference between the following two pathways. The first
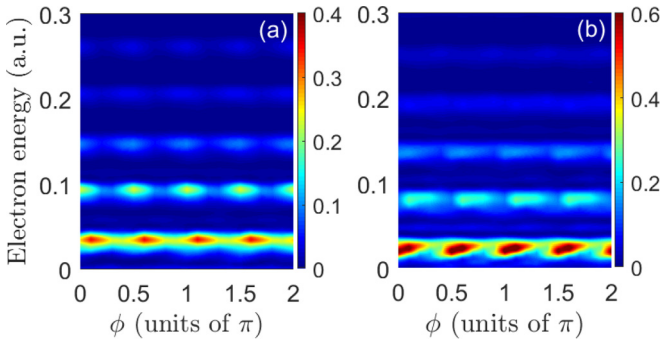
FIG. 7. The ϕ-dependent PES for hydrogen. The laser intensity of the 400-nm field is fixed at $I_1 = 5 \times 10^{13}$ W/cm^2, and the 800-nm fields are (a) $I_2 = 5 \times 10^{12}$ W/cm^2 and (b) $I_2 = 1 \times 10^{13}$ W/cm^2.
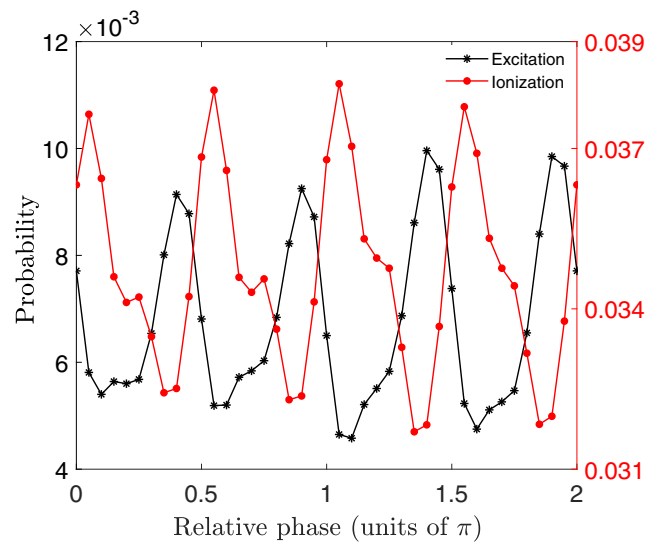

FIG. 8. The probabilities of excitation (black line) and ionization (red line) as a function of relative phase between the two color components. The laser intensities of the 400–800-nm fields are $I_1 = 5 \times 10^{13}$ W/cm^2 and $I_2 = 1.5 \times 10^{13}$ W/cm^2.

pathway is direct ionization of the absorption of five 2ω photons, and the other one is the excitation into excitation state $n = 5$ from the absorption of four 2ω photons and an ω photon, followed by the ionization of further absorbing another ω photon. However, the maximum of the second ATI peak appears at $\phi = n \times \pi/2$. The reason is that the interference of the second ATI peak is mainly from the pathway caused by absorbing five 2ω photons and an ω photon, as well as the ionization from excitation state $n = 5$ caused by absorbing a 2ω photon. When the laser intensity of the 800-nm field increases to $I_2 = 1 \times 10^{13}$ W/cm^2, as shown in the Fig. 7(b), the first ATI peak is enhanced greatly at $\phi = n \times \pi/2$, while the maximum of the second ATI peak changes to $\phi = n \times \pi/2 + 0.1\pi$. The reason is that the excitation channel caused by absorbing three 2ω photons and three ω photons is more pronounced at this intensity. The subsequent ionization introduced by this excitation channel leads to an additional ionization pathway. The interference between these ionization pathways gives rise to the variation of the ϕ-dependent ATI peaks at different intensities of the 800-nm field.

As the 800-nm laser intensity continues to increase, the contribution of the 800-nm field following excitation and ionization becomes more significant. Figure 8 presents the probabilities of excitation and ionization as a function of relative phase when the laser intensity of the 800-nm field increases to $I_2 = 1.5 \times 10^{13}$ W/cm^2. In this case, the probability of ionization is enhanced dramatically by the 800-nm field, and the competition between the excitation and ionization is remarkable. Changing the relative phase of the 400–800-nm fields, the modulation depths Γ of excitation and ionization are 74% and 19%, respectively. We can see that compared with the case with the weaker 800-nm field shown in Figs. 1 and 4, the probabilities' modulation of excitation and ionization with a period of $\pi/2$ is no longer clear at laser intensity $I_2 = 1.5 \times 10^{13}$ W/cm^2. At this point, the ponderomotive energy changes with the variation of the relative phase ϕ. Besides the constructive or destructive interference of different channels, the ponderomotive shift may change the resonant excitation to nonresonant excitation or vice versa. Such a multiphoton (non)resonant transition will certainly change the excitation probability and subsequent ionization, leading to the more complex line structures shown in Fig. 8.

IV. CONCLUSION AND OUTLOOK

We theoretically demonstrated the relative-phase-controlled excitation and ionization of hydrogen atoms using ω-2ω fields. By manipulating the relative phase of the 400–800-nm laser fields, the probabilities of excitation and ionization are controlled by the interference of the different channels. The modulation depth of excitation and ionization is different if we change the laser intensity of the 800-nm field. For laser intensity $I_2 = 5 \times 10^{12}$ W/cm^2, the variations of the excitation and ionization probabilities are almost synchronous with the changing relative phase, and the modulation depths of excitation and ionization are 90% and 42%, respectively. The interference of two excitation channels, i.e., absorbing four 2ω photons and one ω photon and absorbing three 2ω photons and three ω photons, leads to ϕ-dependent excitation and ionization probabilities.

As the laser intensity of the 800-nm laser increases, the contribution from the excitation channel caused by absorbing three 2ω photons and three ω photons is enhanced. The interference produced by the different excitation channels gives rise to the enhancement or suppression of the excitation probability, which can be controlled by tuning the relative phase. In addition, the energy levels of excitation states are shifted by the 800-nm field. It can affect the distribution of nl states and the subsequent ionization, leading to the modulation depths of excitation and ionization changing to 76% and 24% at laser intensity $I_2 = 1 \times 10^{13}$ W/cm^2. When the laser intensity of the 800-nm field increases to $I_2 = 1.5 \times 10^{13}$ W/cm^2, the energy shift from the ac Stark effect is prominent, and more quantum states are involved in the excitation and subsequent ionization. The interference of multiple channels and enhanced ionization make the excitation and ionization processes more complicated. One may expect such a two-color controlled excitation process to be universal and occur in other atoms.

[1] R. Kienberger, E. Goulielmakis, M. Uiberacker, A. Baltuska, V. Yakovlev, F. Bammer, A. Scrinzi, T. Westerwalbesloh, U. Kleineberg, U. Heinzmann, M. Drescher, and F. Krausz, Nature (London) **427**, 817 (2004).

[2] D. Azoury, O. Kneller, S. Rozen, B. D. Bruner, A. Clergerie, Y. Mairesse, B. P. B. Fabre, N. Dudovich, and M. Krüger, Nat. Photon. **13**, 54 (2019).

[3] L. Drescher, T. Witting, O. Kornilov, and M. J. J. Vrakking, Phys. Rev. A **105**, L011101 (2022).

[4] H. Xu, Z. Li, F. He, X. Wang, A. Atia-Tul-Noor, D. Kielpinski, R. T. Sang, and I. V. Litvinyuk, Nat. Commun. **8**, 15849 (2019).

[5] P.-L. He, C. Ruiz, and F. He, Phys. Rev. Lett. **116**, 203601 (2016).

[6] T. Nubbemeyer, K. Gorling, A. Saenz, U. Eichmann, and W. Sandner, Phys. Rev. Lett. **101**, 233001 (2008).

[7] U. Eichmann, T. Nubbemeyer, H. Rottke, and W. Sandner, Nature (London) **461**, 1261 (2009).

[8] R. Borrego-Varillas, M. Lucchini, and M. Nisoli, Rep. Prog. Phys. **85**, 066401 (2022).

[9] Y. Huismans *et al.*, Science **331**, 61 (2011).

[10] G. Porat, G. Alon, S. Rozen, O. Pedatzur, M. Krüger, D. Azoury, A. Natan, G. Orenstein, B. D. Bruner, M. J. J. Vrakking, and N. Dudovich, Nat. Commun. **9**, 2805 (2018).

[11] M. Li, H. Xie, W. Cao, S. Luo, J. Tan, Y. Feng, B. Du, W. Zhang, Y. Li, Q. Zhang, P. Lan, Y. Zhou, and P. Lu, Phys. Rev. Lett. **122**, 183202 (2019).

[12] D. Bauer and P. Koval, Comput. Phys. Commun. **174**, 396 (2006).

[13] H. G. Muller, Laser Phys. **9**, 138 (1999).

[14] H. R. Reiss, Phys. Rev. A **22**, 1786 (1980).

[15] S. V. Popruzhenko and D. Bauer, J. Mod. Opt. **55**, 2573 (2008).

[16] P. J. Kuntz and W. F. Schmidt, J. Chem. Phys. **76**, 1136 (1982).

[17] C. Liu and K. Z. Hatsagortsyan, Phys. Rev. Lett. **105**, 113003 (2010).

[18] H. Jiang and F. He, Phys. Rev. A **104**, 023113 (2021).

[19] M. Li, J.-W. Geng, H. Liu, Y. Deng, C. Wu, L.-Y. Peng, Q. Gong, and Y. Liu, Phys. Rev. Lett. **112**, 113002 (2014).

[20] M. Meyer, D. Cubaynes, D. Glijer, J. Dardis, P. Hayden, P. Hough, V. Richardson, E. T. Kennedy, J. T. Costello, P. Radcliffe, S. Düsterer, A. Azima, W. B. Li, H. Redlin, J. Feldhaus, R. Taïeb, A. Maquet, A. N. Grum-Grzhimailo, E. V. Gryzlova, and S. I. Strakhova, Phys. Rev. Lett. **101**, 193002 (2008).

[21] Y. Fang, C. He, M. Han, P. Ge, X. Yu, X. Ma, Y. Deng, and Y. Liu, Phys. Rev. A **100**, 013414 (2019).

[22] F. Ehlotzky, Phys. Rep. **345**, 175 (2001).

[23] M. Kitzler and M. Lezius, Phys. Rev. Lett. **95**, 253001 (2005).

[24] D. G. Arbó, C. Lemell, S. Nagele, N. Camus, L. Fechner, A. Krupp, T. Pfeifer, S. D. López, R. Moshammer, and J. Burgdörfer, Phys. Rev. A **92**, 023402 (2015).

[25] C. A. Mancuso, D. D. Hickstein, K. M. Dorney, J. L. Ellis, E. Hasović, R. Knut, P. Grychtol, C. Gentry, M. Gopalakrishnan, D. Zusin, F. J. Dollar, X.-M. Tong, D. B. Milošević, W. Becker, H. C. Kapteyn, and M. M. Murnane, Phys. Rev. A **93**, 053406 (2016).

[26] K. J. Schafer and K. C. Kulander, Phys. Rev. A **45**, 8026 (1992).

[27] G. G. Paulus, W. Becker, and H. Walther, Phys. Rev. A **52**, 4043 (1995).

[28] R. M. Potvliege and P. H. G. Smith, J. Phys. B **25**, 2501 (1992).

[29] T. Endo, H. Fujise, H. Hasegawa, A. Matsuda, M. Fushitani, O. I. Tolstikhin, T. Morishita, and A. Hishikawa, Phys. Rev. A **100**, 053422 (2019).

[30] H. Yao, W. Guo, M. R. Hoffmann, and K. Han, Phys. Rev. A **90**, 063418 (2014).

[31] A. D. Bandrauk and S. Chelkowski, Phys. Rev. Lett. **84**, 3562 (2000).

[32] S. Skruszewicz, J. Tiggesbäumker, K.-H. Meiwes-Broer, M. Arbeiter, T. Fennel, and D. Bauer, Phys. Rev. Lett. **115**, 043001 (2015).

[33] L. J. Zipp, A. Natan, and P. H. Bucksbaum, Optica **1**, 361 (2014).

[34] M. Bertolino and J. M. Dahlström, Phys. Rev. Res. **3**, 013270 (2021).

[35] S. Luo, M. Li, H. Xie, P. Zhang, S. Xu, Y. Li, Y. Zhou, P. Lan, and P. Lu, Phys. Rev. A **96**, 023417 (2017).

[36] P. M. Paul, E. S. Toma, P. Breger, G. Mullot, F. Augé, P. Balcou, H. G. Muller, and P. Agostini, Science **292**, 1689 (2001).

[37] Y. Feng, M. Li, S. Luo, K. Liu, B. Du, Y. Zhou, and P. Lu, Phys. Rev. A **100**, 063411 (2019).

[38] S. D. López, S. Donsa, S. Nagele, D. G. Arbó, and J. Burgdörfer, Phys. Rev. A **104**, 043113 (2021).

[39] P. Ge, M. Han, M.-M. Liu, Q. Gong, and Y. Liu, Phys. Rev. A **98**, 013409 (2018).

[40] D. G. Arbó, S. D. López, and J. Burgdörfer, Phys. Rev. A **106**, 053101 (2022).

[41] P. Ge, Y. Dou, M. Han, Y. Fang, Z. Guo, C. Wu, Q. Gong, and Y. Liu, Phys. Rev. A **106**, 053102 (2022).

[42] M. Richter, M. Kunitski, M. Schöffler, T. Jahnke, L. P. H. Schmidt, M. Li, Y. Liu, and R. Dörner, Phys. Rev. Lett. **114**, 143001 (2015).

[43] J.-W. Geng, W.-H. Xiong, X.-R. Xiao, L.-Y. Peng, and Q. Gong, Phys. Rev. Lett. **115**, 193001 (2015).

[44] J. Henkel and M. Lein, Phys. Rev. A **92**, 013422 (2015).

[45] X. Xie, Phys. Rev. Lett. **114**, 173003 (2015).

[46] X. Xie, T. Wang, S. G. Yu, X. Y. Lai, S. Roither, D. Kartashov, A. Baltuška, X. J. Liu, A. Staudte, and M. Kitzler, Phys. Rev. Lett. **119**, 243201 (2017).

[47] M. He, Y. Li, Y. Zhou, M. Li, and P. Lu, Phys. Rev. A **93**, 033406 (2016).

[48] X. Gong, C. Lin, F. He, Q. Song, K. Lin, Q. Ji, W. Zhang, J. Ma, P. Lu, Y. Liu, H. Zeng, W. Yang, and J. Wu, Phys. Rev. Lett. **118**, 143203 (2017).

[49] D. Würzler, N. Eicke, M. Möller, D. Seipt, A. M. Sayler, S. Fritzsche, M. Lein, and G. G. Paulus, J. Phys. B **51**, 015001 (2018).

[50] C. A. Mancuso, K. M. Dorney, D. D. Hickstein, J. L. Chaloupka, J. L. Ellis, F. J. Dollar, R. Knut, P. Grychtol, D. Zusin, C. Gentry, M. Gopalakrishnan, H. C. Kapteyn, and M. M. Murnane, Phys. Rev. Lett. **117**, 133201 (2016).

[51] S. Eckart, M. Richter, M. Kunitski, A. Hartung, J. Rist, K. Henrichs, N. Schlott, H. Kang, T. Bauer, H. Sann, L. P. H. Schmidt, M. Schöffler, T. Jahnke, and R. Dörner, Phys. Rev. Lett. **117**, 133202 (2016).

[52] C. A. Mancuso, K. M. Dorney, D. D. Hickstein, J. L. Chaloupka, X.-M. Tong, J. L. Ellis, H. C. Kapteyn, and M. M. Murnane, Phys. Rev. A **96**, 023402 (2017).

[53] S. Eckart, K. Fehre, N. Eicke, A. Hartung, J. Rist, D. Trabert, N. Strenger, A. Pier, L. P. H. Schmidt, T. Jahnke, M. S. Schöffler, M. Lein, M. Kunitski, and R. Dörner, Phys. Rev. Lett. **121**, 163202 (2018).

[54] J. L. Chaloupka and D. D. Hickstein, Phys. Rev. Lett. **116**, 143005 (2016).

[55] M. Li, W.-C. Jiang, H. Xie, S. Luo, Y. Zhou, and P. Lu, Phys. Rev. A **97**, 023415 (2018).

[56] R. Wang, Q. Zhang, C. Cao, M. Li, K. Liu, and P. Lu, J. Phys. B **55**, 115001 (2022).

[57] N. A. Hart, J. Strohaber, A. A. Kolomenskii, G. G. Paulus, D. Bauer, and H. A. Schuessler, Phys. Rev. A **93**, 063426 (2016).

[58] A. Bunjac, D. B. Popović, and N. S. Simonović, Phys. Chem. Chem. Phys. **19**, 19829 (2017).

[59] B. Piraux, F. Mota-Furtado, P. F. O'Mahony, A. Galstyan, and Y. V. Popov, Phys. Rev. A **96**, 043403 (2017).

[60] S. P. Xu, M. Q. Liu, S. L. Hu, Z. Shu, W. Quan, Z. L. Xiao, Y. Zhou, M. Z. Wei, M. Zhao, R. P. Sun, Y. L. Wang, L. Q. Hua, C. Gong, X. Y. Lai, J. Chen, and X. J. Liu, Phys. Rev. A **102**, 043104 (2020).

[61] Q. Li, X.-M. Tong, T. Morishita, H. Wei, and C. D. Lin, Phys. Rev. A **89**, 023421 (2014).

[62] R. R. Freeman, P. H. Bucksbaum, H. Milchberg, S. Darack, D. Schumacher, and M. E. Geusic, Phys. Rev. Lett. **59**, 1092 (1987).

[63] N. B. Delone and V. P. Krainov, Phys. Usp. **42**, 669 (1999).

[64] D. Chetty, R. D. Glover, B. A. deHarak, X. M. Tong, H. Xu, T. Pauly, N. Smith, K. R. Hamilton, K. Bartschat, J. P. Ziegel, N. Douguet, A. N. Luiten, P. S. Light, I. V. Litvinyuk, and R. T. Sang, Phys. Rev. A **101**, 053402 (2020).

[65] H. Rabitz, R. de Vivie-Riedle, M. Motzkus, and K. Kompa, Science **288**, 824 (2000).

[66] V. Peet and S. Shchemeljov, Phys. Rev. A **68**, 043411 (2003).

[67] H. Bachau, E. Cormier, P. Decleva, J. E. Hansen, and F. Martín, Rep. Prog. Phys. **64**, 1815 (2001).

[68] Z.-H. Zhang, Y. Li, Y.-J. Mao, and F. He, Comput. Phys. Commun. **290**, 108787 (2023).

[69] B. Fetić, W. Becker, and D. B. Milošević, Phys. Rev. A **102**, 023101 (2020).

[70] A. N. Grum-Grzhimailo, A. D. Kondorskiy, and K. Bartschat, J. Phys. B **39**, 4659 (2006).

[71] T. Nakajima and S. Watanabe, Phys. Rev. Lett. **96**, 213001 (2006).

[72] D. Chetty, R. D. Glover, X. M. Tong, B. A. deHarak, H. Xu, N. Haram, K. Bartschat, A. J. Palmer, A. N. Luiten, P. S. Light, I. V. Litvinyuk, and R. T. Sang, Phys. Rev. Lett. **128**, 173201 (2022).

[73] Z. Chen, T. Morishita, A.-T. Le, M. Wickenhauser, X. M. Tong, and C. D. Lin, Phys. Rev. A **74**, 053405 (2006).

[74] P. Wang and H. Feng, Chin. Phys. B **18**, 5291 (2009).

[75] U. Fano, Phys. Rev. A **32**, 617 (1985).

[76] D. Busto, J. Vinbladh, S. Zhong, M. Isinger, S. Nandi, S. Maclot, P. Johnsson, M. Gisselbrecht, A. L'Huillier, E. Lindroth, and J. M. Dahlström, Phys. Rev. Lett. **123**, 133201 (2019).